35th Annual International Conference of the IEEE EMBS
Osaka, Japan, 3 - 7 July, 2013

Automated Anterior Chamber Angle Localization and Glaucoma Type Classification in OCT Images*

Yanwu Xu, Jiang Liu, Jun Cheng, Beng Hai Lee, Damon Wing Kee Wong,
Baskaran Mani, Shamira Perera and Tin Aung

***Abstract*— To identify glaucoma type with OCT (optical coherence tomography) images, we present an image processing and machine learning based framework to localize and classify anterior chamber angle (ACA) accurately and efficiently. In digital OCT photographs, our method automatically localizes the ACA region, which is the primary structural image cue for clinically identifying glaucoma type. Next, visual features are extracted from this region to classify the angle as open angle (OA) or angle-closure (AC). This proposed method has three major contributions that differ from existing methods. First, the ACA localization from OCT images is fully automated and efficient for different ACA configurations. Second, it can directly classify ACA as OA/AC based on only visual features, which is different from previous work for ACA measurement that relies on clinical features. Third, it demonstrates that higher dimensional visual features outperform low dimensional clinical features in terms of angle closure classification accuracy. From tests on a clinical dataset comprising of 2048 images, the proposed method only requires 0.26s per image. The framework achieves a 0.921 ± 0.036 AUC (area under curve) value and $84.0\% \pm 5.7\%$ balanced accuracy at a 85% specificity, which outperforms existing methods based on clinical features.**

I. Introduction

Glaucoma is a group of heterogeneous optic neuropathies characterized by the progressive loss of axons in the optic nerve. Data from the World Health Organization shows that glaucoma accounts for 5.1 million cases of blindness in the world and is the second leading cause of blindness worldwide (behind cataracts) as well as the foremost cause of irreversible blindness [1]. As illustrated in Fig. 1, *glaucoma is classified according to the configuration of the angle* (the part of the eye between the cornea and iris mainly responsible for drainage of aqueous humor) into open angle (OA) and angle-closure (AC) glaucoma.

Primary angle closure glaucoma (PACG) is a major form of glaucoma in Asia [2] compared to primary open angle glaucoma (POAG), which is more common in Caucasians and Africans [3]. PACG is already responsible for the majority of bilateral glaucoma blindness in Asia, which will affect 20 million people. Previously reported anatomical risk factors for angle closure include a shallow central anterior chamber depth (ACD), a thick and anterior lens position and short axial length (AL) [4]. Amongst these, a shallow ACD is regarded as a sine qua non (cardinal risk factor) for the disease. However, population based data suggest that only a small proportion of subjects with shallow ACD ultimately develop PACG [5]. Therefore, it is likely that other ocular factors relate to PACG development and need to be discovered.

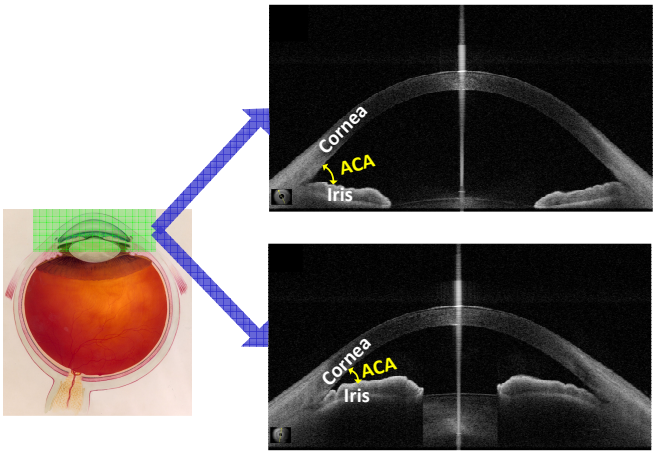

Fig. 1. Open angle (OA, top) and angle-closure (AC, bottom).

In previous work, automated glaucoma type classification has been studied in different image modalities. A BIF feature based learning method was proposed for color RetCam images [6]. An edge detection and line fitting approach was proposed for ACA measurement [7] in ultrasound biomicroscopy (UBM) images. Similarly, a segmentation, edge detection and linear regression based approach was proposed for ACA assessment in OCT images [8].

In this work, we study ACA localization and classification for glaucoma type identification in OCT (optical coherence tomography) images, which has the advantages of being non-invasive and non-contact [9] compared to UBM. An OCT image captures a cross-section of the eye as a grayscale image, and several features (as illustrated in Fig. 2) are extracted based on ACA measurement such as AOD (angle-opening distance) [7], [8], TIA (trabecular-iris angle) [10], TISA (trabecular–iris space area) [8], [10] and SLBA (Schwalbe's line bounded area) [11]. In practice, these clinical features are used for angle closure assessment, *i.e.*, ACA classification.

ACA detection in OCT images can be relatively straight-

*This work was supported in part by the Agency for Science, Technology and Research, Singapore, under BMRC grant 10/1/35/19/674.

Y. Xu, J. Liu, J. Cheng, B. H. Lee and D.W.K. Wong are with the Institute for Infocomm Research, Agency for Science, Technology and Research, 138632, Singapore {yaxu, jliu, jcheng, benghai, wkwong} at i2r.a-star.edu.sg

M. Baskaran, S.A. Perera and T. Aung are with the Singapore Eye Research Institute, 168751, Singapore baskaran.mani at seri.com.sg, shamira.perera at snec.com.sg, aung.tin at snec.com.sg

T. Aung is also with the Department of Ophthalmology, National University of Singapore, 119074, Singapore

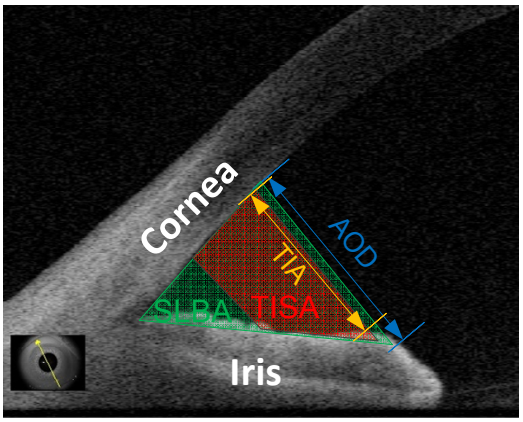

Fig. 2. Features used for ACA measurement clinically. Please refer to the color print for better viewing.

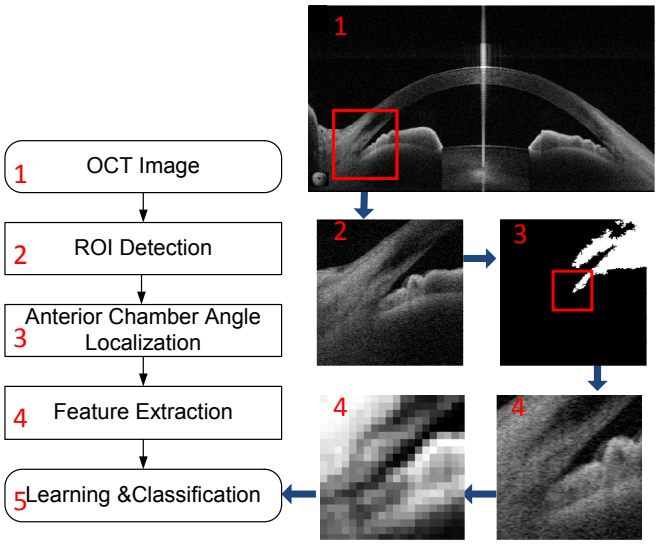

Fig. 3. Flowchart of the proposed ACA localization and classification.

forward since the images are generally clean and are approximately aligned during image acquisition process. However, ACA classification is a challenging task since there are intermediate cases that are difficult to classify as AC or OA using the same clinical features, even for human experts. From our image classification experience, the use of only one or two dimensional clinical features is insufficient to achieve good performance, since the eigen dimension of this problem might be much higher, *as observed clinically* [5].

In this paper, we propose an image processing and learning based framework for efficient ACA localization and classification. With the proposed framework, other existing visual features and learning algorithms can be introduced to improve performance in the future.

II. Angle Closure Classification

To classify an ACA as open or closed, a natural solution is to follow the method of a human expert. Generally, as shown in Fig. 3, for a given OCT image, the ACA region needs to be localized accurately at first, and then certain features and criteria are used to identify whether it is closed.

A. ACA localization

In previous work, the ACA regions are marked manually [10] or are automatic determined by using edge detection [7]. For efficiency, we adopt a coarse-to-fine scheme to localize the ACA from input OCT image, which first segments a candidate ACA region and then localizes its vertex for alignment. The steps are shown in Fig. 3. First, a 400×400 region of interest (ROI) covering the exact ACA is cropped out at a fixed position from the 834×900 input image; second, the ROI is quantized to a binary image (0 for black and 1 for white) using a small valued threshold in order to preserve more details of the angle (a large/adaptive threshold will lose more details at the extreme end of the ACA, which is very important for classification); third, a morphological operation is performed to remove isolated noise points; fourth, weighting and connected component labeling segmentation (CCLS) [8] algorithm are used to segment the ACA candidate in the ROI; fifth, a post processing step is applied to remove other components connected to the exact ACA in the candidate region; lastly, the ACA is localized with an $n \times n$ bounding box centered at its detected vertex. For further details, readers are referred to our recent work [12].

B. ACA feature representation and classification

Each ACA region is represented by a $n \times n$ image, which can be grayscale, binary and/or edges of the ACA. Many existing features from computer vision can be used for classification, such as HOG [13] and BIF [6] which are related to edges and textures, respectively.

In this work, we use the histogram equalized pixel (HEP) values as a feature that is effective and computationally efficient. This is motivated by the intensity of a pixel being a natural feature [14] to classify whether it is on a closed angle. However, using all the pixels in the $n \times n$ region will generate features that are too high dimensional and may also introduce too much noise. Therefore, we downsample the image to reduce the feature dimension. The additional quantization with fewer bins before downsampling enhances the contrast between pixels and provides more distinguishable features.

As illustrated in Fig. 4, the $n \times n$ grayscale image of ACA is first enhanced by quantizing to 8 bins, and then downsampling to $d \times d (d < n)$, so that the vectored image $\mathbf{f}$ is the HEP feature. For efficiency, the simple linear SVM classifier is employed, with a weight vector ω trained to estimate the class label y (+1 for AC and -1 for OA) of a given feature vector $\mathbf{f}$, according to $y = \omega^T \mathbf{f}$. In the experiments, we use the LIBLINEAR toolbox [15] to train the SVM models.

III. Experiments

A. Experimental setup

Our approach is implemented with Matlab and tested on a four-core 3.4GHz PC with 12GB RAM. A total of 2048

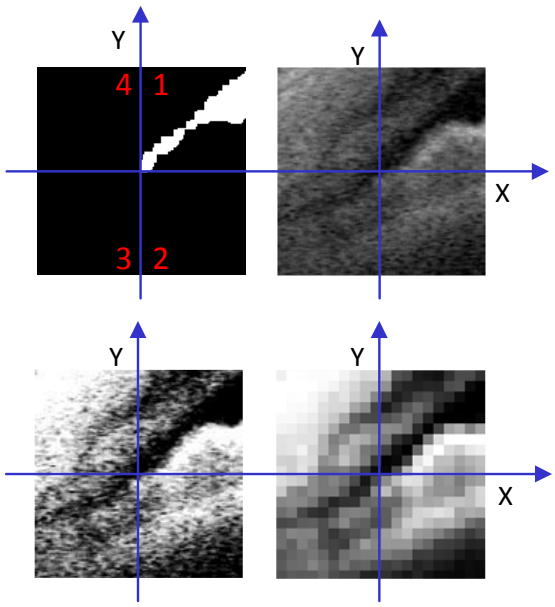

Fig. 4. ACA feature representations (left top to right bottom): binary, grayscale, histogram equalized and HEP.

images are used for the experiments. The images are from 8 circular scan videos of 8 patient eyes with glaucoma, 4 of them with PACG and other 4 with POAG. Each video contains 128 frames, and each frame is split into 2 images since it contains two angles and the right angle image is flipped horizontally.

The experiments are based on each single image, which is labeled as AC or OA by three ophthalmologists from a hospital. For the classification evaluation, we follow the widely used leave-one-out (LOO) method, *i.e.*, for each testing round, 512 images from one PACG and one POAG patients are used for testing while others are used for training, thus 16 rounds are performed to test all cases.

We assess the performance using a balanced accuracy with a fixed 85% specificity and area under ROC curve (AUC) *which evaluates the overall performance*. The balanced accuracy ($\bar{P}$), sensitivity (P_+) and specificity (P_-) are defined as

$$\begin{aligned} \bar{P} &= \frac{P_+ + P_-}{2}, \\ P_+ &= \frac{TP}{TP+FN}, \\ P_- &= \frac{TN}{TN+FP}, \end{aligned} \tag{1}$$

where TP and TN denote the number of true positives and negatives, respectively, and FP and FN denote the number of false positives and negatives, respectively.

B. Comparison of ACA classification

In this section, we compare classification methods with several visual features (*i.e.*, BIF [6], HOG [13] and HEP) with different ACA region sizes ($n = 100, 150, 200$) and two clinical features (*i.e.*, AOD [8] and SLBA [11]). For the HEP feature extraction, d is set to 20 for efficiency reasons.

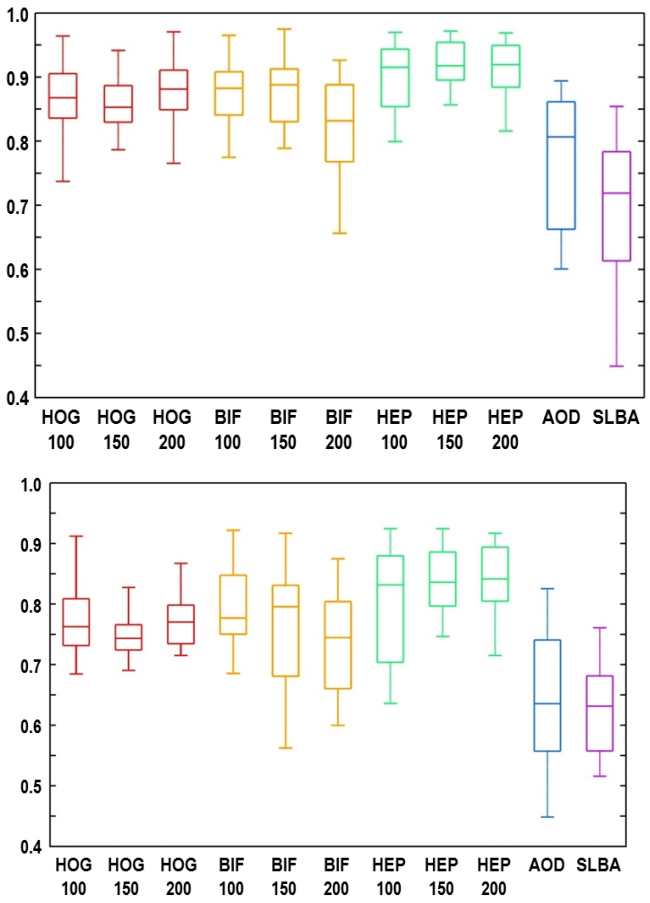

Fig. 5. Performance comparison in terms of AUC (top) and balanced accuracy (bottom).

For HOG and BIF feature extraction, the ACA is divided into 5×5 cells; 2×2 cells form a block for HOG, and 22 feature maps are used for BIF. From the results shown in Fig. 5 and Table I, we have the following observations:

1) The visual feature based methods outperform the clinical feature based ones, demonstrating that high dimensional visual features provide more information for classification and thus leading to higher performance. In addition, the performance drops significantly in some videos that contains a lot of intermediate cases which are difficult to classify even for human experts.
2) Among visual feature based methods, the simplest HEP features outperform HOG and BIF features. A possible explanation is that HOG features introduces noise and BIF is not very suitable for grayscale images.
3) Comparing methods based on the HEP feature with different ACA size n, the results are relatively stable, and the largest AUC is obtained when setting $n = 150$, which was found to be not too small to lose useful information nor too big to introduce too much noises.

We also observed that histogram equalization can lead to about 2–3% relative improvement of AUC compared to downsampling only. In terms of processing speed, each

TABLE I

PERFORMANCE COMPARISONS OF ACA CLASSIFICATION WITH DIFFERENT FEATURES

Feature	HOG			BIF			HEP			AOD	SLBA
n	100	150	200	100	150	200	100	150	200	–	–
AUC	0.865 $\pm$0.058	0.847 $\pm$0.063	0.882 $\pm$0.054	0.877 $\pm$0.054	0.872 $\pm$0.078	0.821 $\pm$0.080	0.899 $\pm$0.059	**0.921 $\pm$0.036**	0.914 $\pm$0.045	0.745 $\pm$0.166	0.697 $\pm$0.108
$\bar{P}(\%)$	76.2 $\pm$7.6	76.0 $\pm$5.6	78.5 $\pm$6.6	79.3 $\pm$7.1	76.8 $\pm$11.0	73.6 $\pm$8.5	80.2 $\pm$9.9	84.0 $\pm$5.7	**84.2 $\pm$6.0**	63.9 $\pm$11.7	62.1 $\pm$7.5

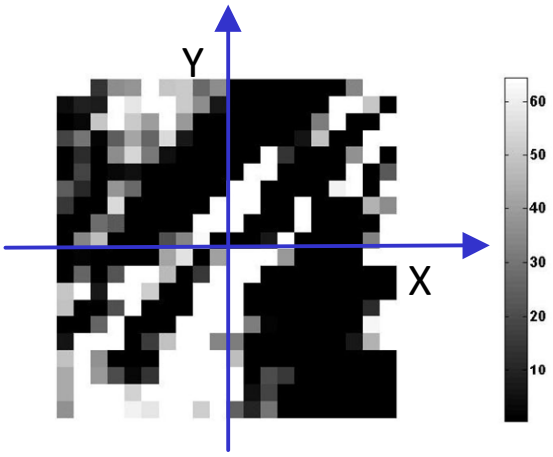

Fig. 6. The learned average weight matrix.

ACA represented by a 400-dimension feature costs about 0.06s for feature extraction and classification with a Matlab implementation, which can be further accelerated with a C++ implementation.

In addition, we found a way to further reduce the feature dimension without significant reduction of accuracy. As shown in Fig. 4, with the proposed ACA localization, each ACA is aligned with its vertex at the center, and then the exact ACA should fall into quadrant 1; however, some ACAs are misaligned since the exact vertex of an ACA is very hard to distinguish when that region is blurred. In this case, the extreme ends of some ACA corners fall into quadrant 3, especially for closed ones. Thus we suppose that quadrant 1 and 3 may provide sufficient information for classification, which is supported by experiments. The average weight vectors $\bar{\omega}$ we obtained in the testing are illustrated in Fig. 6; for each dimension (shown as a block), a higher weight corresponds to a lighter color. One can observe that most of the dimensions with highest weights (in white) are in quadrant 1 and 3, as expected. Thus the performance of using all of the $d \times d$ pixels was compared with only using pixels in quadrants 1 and 3, the AUC reduction is less than 0.3% with a half dimension reduction.

IV. CONCLUSION

For glaucoma type identification, an image processing and machine learning based framework was proposed to localize and classify ACA accurately and efficiently, based on visual features only. We tested our method on a clinical dataset comprised of 2048 images with two evaluation criteria. The results show that it outperforms clinical feature based methods, achieving a 0.921 ± 0.036 AUC value and $84.0\% \pm 5.7\%$ balanced accuracy ($\bar{P}$) at a 85% specificity (P_{-}), while only requiring 0.26s per image. In future work, we plan to extend the classification framework to multiple level angle closure grading, in order to improve precision and better deal with intermediate cases.

REFERENCES

[1] B. Thylefors, A.D. Negrel, R. Pararajasegaram, and K.Y. Dadzie, "Global data on blindness," *Bull WHO*, vol. 73, no. 1, pp. 115–21, 1995.

[2] P.J. Foster and G.J. Johnson, "Glaucoma in china: how big is the problem?," *Br J Ophthalmol*, vol. 85, pp. 1277–82, 2001.

[3] B.E. Klein, R. Klein, W.E. Sponsel, T. Franke, L.B. Cantor, J. Martone, and Menage M.J., "Prevalence of glaucoma. the beaver dam eye study," *Ophthalmology*, vol. 99, pp. 1499–504, 1992.

[4] N.G. Congdon, Q. Youlin, H. Quigley, T.H. Hung, P.T.and Wang, T.C. Ho, and J.M. Tielsch, "Biometry and primary angle-closure glaucoma among chinese, white, and black populations," *Ophthalmology*, vol. 104, pp. 1489–95, 1997.

[5] N.L. Wang, H.P. Wu, and Z.G. Fan, "Primary angle closure glaucoma in chinese and western populations," *Chinese Medical Journal*, vol. 115, pp. 1706–15, 2002.

[6] J. Cheng, D. Tao, J. Liu, D.W.K. Wong, B.H. Lee, M. Baskaran, T.Y. Wong, and T. Aung, "Focal biologically inspired feature for glaucoma type classification," in *MICCAI*, 2011, vol. 6893, pp. 91–8.

[7] W.H. Leung, C.K.and Yung, C.K. Yiu, S.W. Lam, D.Y. Leung, R.K. Tse, C.C. Tham, W.M. Chan, and D.S. Lam, "Novel approach for anterior chamber angle analysis: anterior chamber angle detection with edge measurement and identification algorithm (academia)," *Arch Ophthalmol*, vol. 124, no. 10, pp. 1395–401, 2006.

[8] J. Tian, P. Marziliano, M. Baskaran, H.T. Wong, and T. Aung, "Automatic anterior chamber angle assessment for hd-oct images," *IEEE Transactions on Biomedical Engineering*, vol. 58, no. 11, pp. 3242–9, 2011.

[9] C.K. Leung, C.Y. Cheung, H. Li, S. Dorairaj, C.K. Yiu, A.L. Wong, J. Liebmann, R. Ritch, R.N. Weinreb, and D.S. Lam, "Dynamic analysis of darklight changes of the anterior chamber angle with anterior segment oct," *Invest Ophthalmol Vis Sci*, vol. 48, no. 9, pp. 4116–22, 2007.

[10] C.K. Leung, R.N. Weinreb, j. Liu, C.Y. Cheung, R.Y. Lai, C.P. Pang, and D.S. Lam, "Anterior chamber angle measurement with anterior segment optical coherence tomography: A comparison between slit lamp oct and visante oct," *Invest. Ophthalmol. Vis. Sci.*, vol. 49, no. 8, pp. 3469–74, 2008.

[11] J. Tian, P. Marziliano, and H.T. Wong, "Automatic detection of schwalbe's line in the anterior chamber angle of the eye using hd-oct images," in *EMBC*, 2010, pp. 3013–6.

[12] Y. Xu, J. Liu, N.M. Tan, B.H. Lee, D.W.K. Wong, S. Baskaran, M. amd Perera, and T. Aung, "Anterior chamber angle classification using multiscale histograms of oriented gradients for glaucoma subtype identification," in *EMBC*, 2012.

[13] N. Dalal and B. Triggs, "Histograms of oriented gradients for human detection," in *CVPR*, 2005, vol. 1, pp. 1886–93.

[14] M.J. Gangeh, L. Sørensen, S.B. Shaker, M.S. Kamel, M. de Bruijne, and M. Loog, "A texton-based approach for the classification of lung parenchyma in ct images," in *MICCAI*, 2010, vol. 6363, pp. 595–602.

[15] R.E. Fan, K.W. Chang, C.J. Hsieh, X.R. Wang, and C.J. Lin, "LIBLINEAR: A library for large linear classification," *Journal of Machine Learning Research*, vol. 9, pp. 1871–4, 2008.